Journal of
Materials Chemistry C

Accepted Manuscript

This article can be cited before page numbers have been issued, to do this please use: P. Chen, G. Liu, H. Zhang, M. Jin, M. Han, Z. Cheng, Q. Peng, Q. Li and Z. Li, *J. Mater. Chem. C*, 2018, DOI: 10.1039/C8TC01598H.

ROYAL SOCIETY OF CHEMISTRY

rsc.li/materials-c

View Article Online
DOI: 10.1039/C8TC01598H

Journal Name

ARTICLE

Rigid Ringlike Molecule: Large Second-Order Nonlinear Optical Performance, Good Temporal and Thermal Stability, and Ideal Spherical Structure Conforming the "Site Isolation" Principle

Received 00th January 20xx,
Accepted 00th January 20xx

DOI: 10.1039/x0xx00000x

www.rsc.org/

Pengyu Chen, [a] Guangchao Liu, [a] Huanyu Zhang, [a] Meng Jin, [a] Mengmeng Han,[a] Ziyao Cheng, [a] Qian Peng,[b] Qianqian Li, [a] and Zhen Li*,[a]

In this paper, according to the principle of site isolation, a ringlike molecule of **R1**, based on the second-order nonlinear optical chromophore of FTC (Fang's Thermally-Stable Chromophore), was designed and synthesized, in which, the heads and waists of two FTC moieties were locked together through chemical bonds, respectively. Thanks to the ideal spherical structure and good alignment of the two pieces of FTC moieties, **R1** exhibited the ultra high nonlinear optical effect with the d_{33} value of 562 pm V^{-1} at the wavelength of 1950 nm, which could still keep 80% at a very high temperature of 145 °C.

Introduction

With the development of information technology in the past decades, humans' demand for the related high performance devices increased rapidly, such as ultrafast optical switches, high-speed optical modulators, high-density optical data storage and so on. Hence, accordingly, second-order nonlinear optical (NLO) materials have attracted considerable interest. Compared to conventional inorganic crystalline materials, organic NLO materials possess some advantages, including the good processability, ultrafast response time and superior chemical flexibility. [1]

To achieve the required macroscopic NLO performance, the chromophore moieties should be aligned orderly in non-centrosymmetry, then, the large microscopic β values of the chromophore moieties could be translated into high macroscopic NLO activities of NLO polymers effectively. However, the strong dipole-dipole interactions between the chromophore moieties with the donor-π-acceptor (D-π-A) structure always hinder this orderly alignment even during the poling process under an electric field with the high voltage, but relax it to the centrosymmetric state upon the removal of the electric field or the raise of temperature.[2] Thus, lots of works have been conducted to solve this problem with some success, while in some cases, other problems arouse, for example, the optical transparency, thermal and photo stability, and temporal stability. [3] Actually, it is still a big problem nowadays in this research area, that how to reduce the dipole-dipole interactions between the chromophore moieties and overcome the motion of chromophore moieties after poling. Generally, according to the "site isolation" principle proposed by Dalton, the spherical structure of chromophore could effectively decrease the dipole-dipole interactions.[4] Furthermore, as pointed out by the concept of "suitable isolation group" (SIG), if isolation groups with suitable size were attached to the chromophore moieties, the balance between the reduced dipole-dipole interactions and the decreased loading density of the chromophore moieties could be realized, to achieve the large NLO performance as high as possible.[5]

Considering all the above points, in this paper, a rigid ringlike molecule based on FTC chromophore of **R1** was designed and synthesized, as shown in Figure 1. This special design molded two FTC moieties into an idea spherical structure, in which, the heads and waists of two chromophores were locked together through chemical bonds, respectively. This ideal spherical structure would not be changed easily and the intermolecular dipole-dipole interaction could be decreased efficiently. Besides, due to the constraint of them, the two FTC moieties had almost

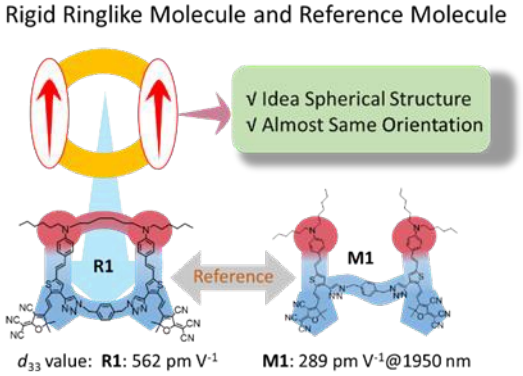

Fig. 1 Rigid ringlike molecule and its reference molecule.

[a] Department of Chemistry, Hubei Key Lab on Organic and Polymeric Opto-Electronic Materials, Wuhan University, Wuhan 430072, China. E-mail: lizhen@whu.edu.cn or lichemlab@163.com.
[b] Key Laboratory of Organic Solids, Beijing National Laboratory for Molecular Science Institute of Chemistry, Chinese Academy of Sciences, Beijing 100190, China

Electronic Supplementary Information (ESI) available: [details of any supplementary information available should be included here]. See DOI: 10.1039/x0xx00000x

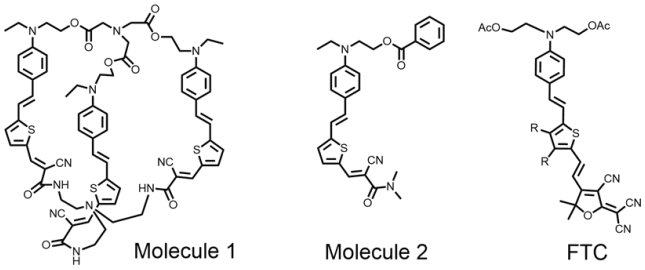

β values HRS
(×10^{-30} esu): 237 @1.3 μm 97 @1.3 μm 635 @1.9 μm

Fig. 2 Macrocyclic trichromophore bundle and two chromophore.

the same orientation, which was beneficial to the translation from microscopic *β* value to macroscopic NLO activity. A similar molecule without ringlike structure, **M1**, was also synthesized for comparison. Herein, we would like to present the synthesis, characterization, thermal stability, optical and NLO properties of the rigid ringlike molecule of **R1** and the reference molecule of **M1** in detail. Besides, related data of pure FTC chromophore were also listed for comparison.

View Article Online
DOI: 10.1039/C8TC01589H

Results and discussion

Molecular Design, Synthesis and Characterization

The key point to overcome the motion of chromophore moieties after poling was to restrict the movement of chromophore moieties.[6] Accordingly, the locking of more than one pieces of chromophore moieties together should be one of the most effective approach. Thus, a very simple structure, rigid ringlike molecule of **R1** was designed, with the structure shown

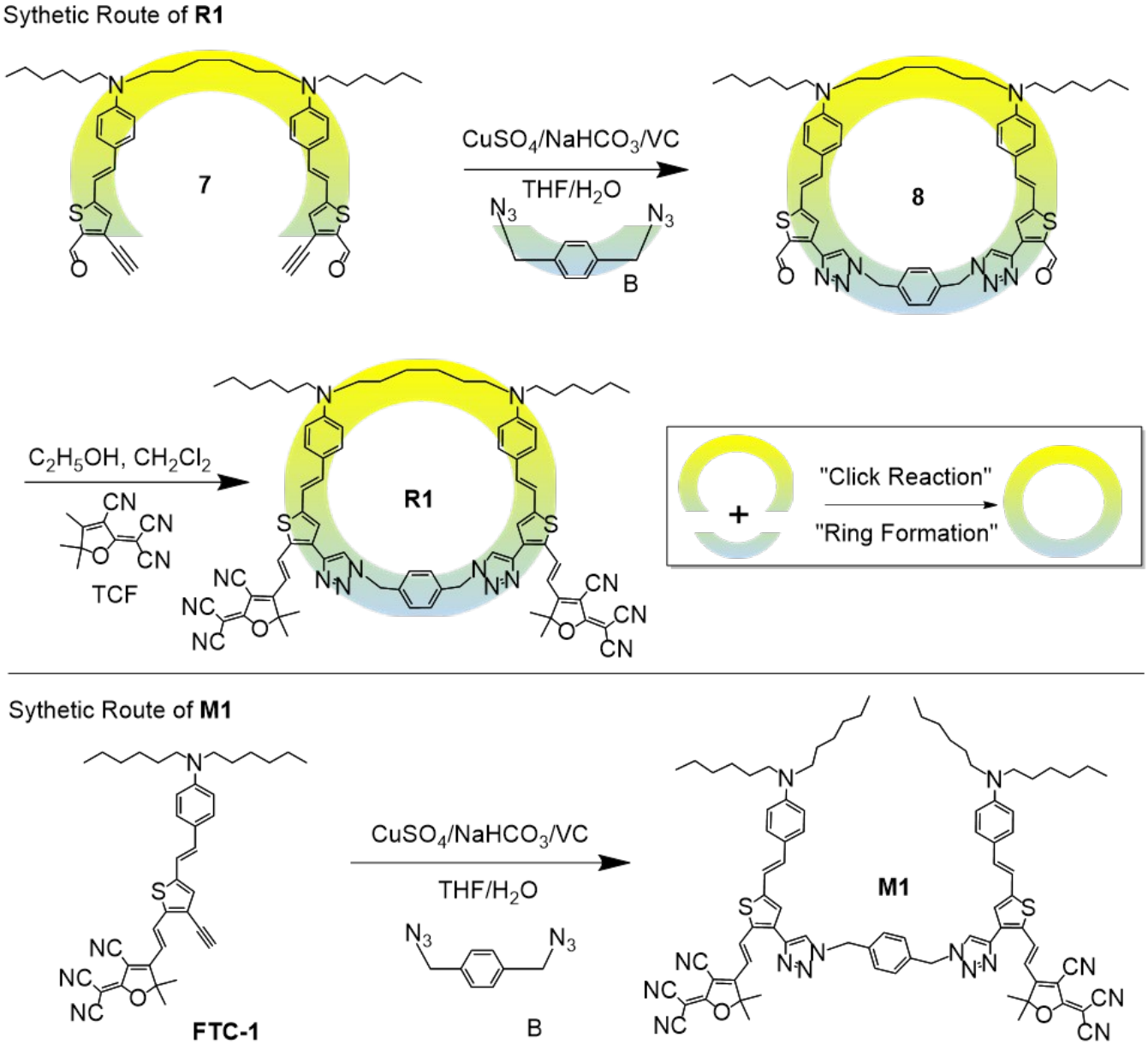

Fig. 3 Synthetic routes of **R1** and **M1**.

View Article Online
DOI: 10.1039/C8TC01598H

Figure 1, in which two FTC moieties were locked in the two points of head and waist.

Actually, in 2006, a macrocyclic trichromophore bundle was designed, in which, the heads and tails of three chromophore moieties were locked together through chemical bonds, respectively (Figure 2).[7] This constraint made the three chromophore moieties have parallel-aligned dipole moments, and the microscopic β value increased a lot (β value of molecule 1 was 237×10^{-30} esu and that of molecule 2 was only 97×10^{-30} esu). However, the microscopic β value of molecule 1 was still very low, limiting the possible industrial applications. And it was a pity that no macroscopic NLO activity was reported.

Here, FTC chromophore with very large microscopic β value (about 635×10^{-30} esu) was chosen to synthesize the ringlike molecule.[8] Because of the strong TCF acceptor, FTC chromophore had a very large dipolar moment (13 D), which hindered the formation of the ring and increased the synthetic difficulty largely.[8] Thus, as shown in Figure 3 and Figure S11, the synthetic process of the ringlike molecule of **R1** was started from the donor-pair part, and two aniline groups were connected easily through a (-C_6H_{12}-) carbon chain. Accordingly, the special donor was obtained from the reaction of compound **1** with 1-bromohexane. After the followed Vilsmeier, Wittig, Sonogashira and another Vilsmeier reactions, compound **7**, the important reactive intermediate for the Ring-Formation reaction, was obtained. Although the aldehyde groups were not strong withdrawing ones and the powerful Click Chemistry Reaction was used, the yield of Compound **8** was very low as only 16.6%, indicating the synthetic difficulty possibly due to the dipole-dipole interactions. Initially, the compound **9** (Figure S11), with the similar structure to compound **5** but without trimethylsilyl groups, was used as the reactant for the ring formation reaction to synthesize compound **10**, because of its weak dipolar moment. Unfortunately, the target product was not obtained. Some suspected product went bad rapidly in the purification process. It seemed that compound **10** was easily oxidized in air. After the two terminal alkynes were bonded together, the target molecule of **R1** was yielded successfully through the Knoevenagel condensation reaction between Compound **8** and TCF. For comparison, the reference molecule of **M1** was synthesized similarly through the Click reaction by linking two pieces of FTC-1 together. **M1** had a similar structure to **R1**, with the minor difference in the unlocked donor part. **R1** and **M1** were well characterized by nuclear magnetic resonance (NMR) (Figure 4, Figure S8), infrared spectroscopy (IR) (Figure 4, Figure S4), thermogravimetric analysis (TGA) (Figure S2), ultraviolet-visible spectroscopy (UV-vis) (Figure S5), differential scanning calorimetry (DSC) (Figure S3), elemental analyses (EA), and matrix-assisted laser desorption ionization-time of flight-mass spectrometry (MALDI-TOF-MS) (Figure 4, Figure S9).

In the synthetic route of **R1** (Figure 3 and Figure S11), Compound **7** had two aldehyde groups and two terminal alkyne groups, and Compound **8** had two aldehyde groups and two triazole groups but no terminal alkyne groups, while no aldehyde groups and terminal alkyne groups in **R1**. Accordingly, as shown in Figure 4A, at about 3.5 ppm, there was one peak (2 ≡CH) in the ^{1}H NMR spectrum of Compound **7**, while there were no peaks in ^{1}H NMR spectra of Compound **8** and **R1**. While at

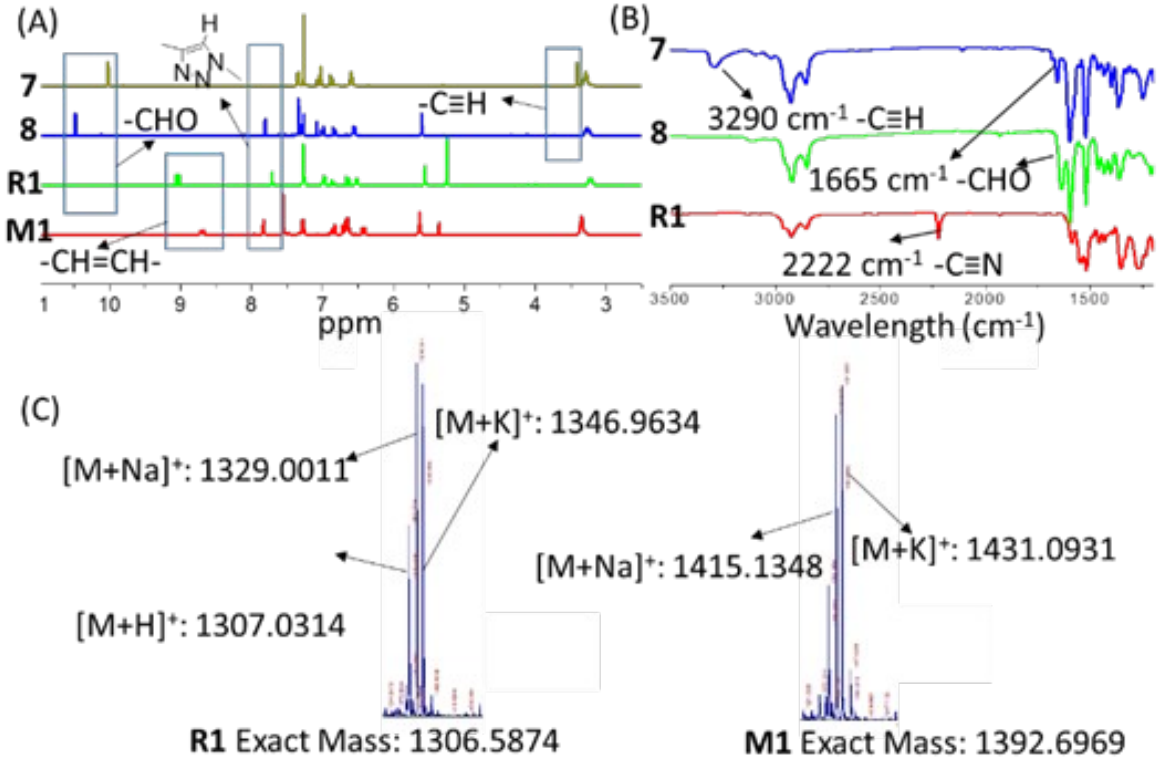

Fig. 4 (A) 1H NMR of some intermediate products and destination product **R1** and **M1**; (B) IR spectra of Compound **7**, **8** and **R1**; (C) TOF spectra of **R1** and **M1**.

about 10.5 ppm, there was one peak (2 -CHO) in the ^{1}H NMR spectra of Compound **7** and Compound **8**, there were no peaks in the ^{1}H NMR spectrum of **R1**, confirming the successful Click Chemistry and Knoevenagel condensation reactions. It was worth noting that the peak of aldehyde groups of Compound **7** was at 10.02 ppm, while that of Compound **8** was at 10.47 ppm. Meantime, in the ^{1}H NMR spectrum of **R1**, the peak of ethylenic bonds, which were close to TCF acceptors, was at about 9.05 ppm, while that of **M1** was at about 8.67 ppm. These differences also proved that "Ring" structures existed in the two molecules of Compound **8** and **R1**.

Some typical groups could be easily detected by Infrared spectroscopy, such as azido groups (near 2900 cm^{-1}), terminal alkyne (near 3100 cm^{-1}), aldehyde groups (near 1700 cm^{-1}), and cyano groups (near 2220 cm^{-1}). As shown in Figure 3, Compound **8** was synthesized through the "cyclization-click chemistry" reaction between Compound **7** and Compound B. Then **R1** was obtained through the Knoevenagel Condensation between Compound **8** and TCF. Thus, in the screenshot of IR spectra of Compound **7**, **8** and **R1** (Figure 4B), obviously, the peak of terminal alkyne groups (3290 cm^{-1}) could be found for Compound **7**, but disappeared in that of Compound **8**, demonstrating the successful click chemistry reaction once again. In the IR spectrum of **R1**, there were no peaks at 1665 cm^{-1}, proving the complete reaction of the aldehyde groups, while the peak appearing at 2222 cm^{-1} confirmed the successful linkage of TCF acceptor containing cyano groups through the Knoevenagel condensation reaction. MALDI-TOF-MS is a powerful tool to characterize molecules with high molecular weights. For the large polarity of these two molecules, sodium ionization and potassium ionization were adopted. As shown in Figure 4(C) and Figure S9, the peaks at 1307.0314, 1329.0011 and 1346.9634 belonged to $[M+H]^+$, $[M+Na]^+$ and $[M+K]^+$ of **R1** and the peaks at 1415.1348 and 1431.0931 should be ascribed to $[M+Na]^+$ and $[M+Na+K]^+$ of **M1**, which could undoubtedly confirm the successful synthesis of **R1** and **M1**.

Thermal properties

The TGA curves of **M1** and **R1** were shown in Figure S2. Both of them possessed very good thermal stability, with the decomposition temperatures (T_d) (temperatures for 5% weight loss) of 266 and 277 °C respectively (Table 1), which were higher than 260 °C (the decomposition temperature of original FTC chromophore). Relatively, it could be found that there was a slight decrease (11 °C) for the thermal stability of **R1**, indicating that the formation of the ring did not cause large damage to the molecular stability. The glass transition temperature (T_g) was another important thermal property. It was related to the poling process (Figure S1). The chromophore moieties could move to some degree at a similar or higher temperature than T_g to achieve the required orderly alignment, so the difficulty of poling and the best poling temperature were heavily related to it. From the DSC curve (Figure S3), the glass transition temperature (T_g) of **M1** was 104 °C, (Table 1). However, the glass transition temperatures (T_g) of **R1** and pure FTC chromophore could not be obtained.

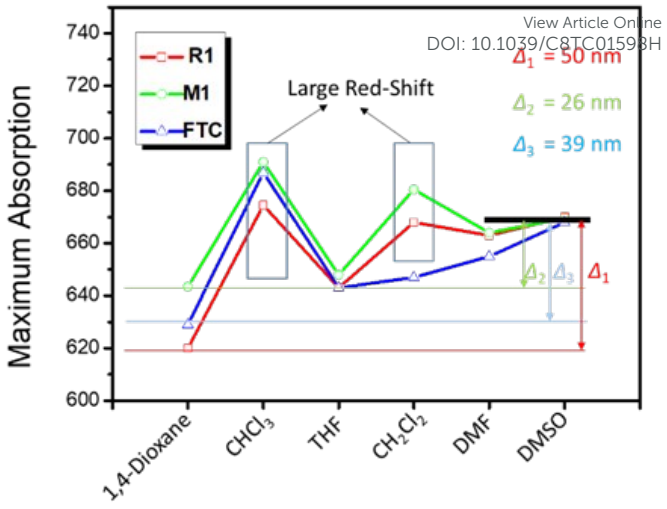

Fig. 5 Solvatochromism spectra of **R1**, **M1** and pure FTC chromophore.

Optical properties

The UV-vis absorption spectra of **R1**, **M1** and pure FTC chromophore in different solvents were shown in Figure S5, with their maximum absorption (λ_{max}) wavelengths summarized in Figure 5 and Table 1. Also, the corresponding data of pure FTC chromophore was measure and listed for comparison. Due to the presence of FTC moieties, all the maximum absorption wavelengths existed at about 660 nm in UV-vis absorption spectra. Theoretically, the λ_{max} would red-shift in accordance with the enhancement of the polarity of solvent. As for the pure FTC chromophore, the λ_{max} in $CHCl_3$ was the longest in the six solvents, and the same phenomena existed in the spectra of **R1**

Table 1 Thermal properties, NLO performance and solvatochromism results of two compounds and pure FTC chromophore.

NO.	T_g[a] (°C)	T_d[b] (°C)	T_e[c] (°C)	$T_{80\%}$[d] (°C)	d_{33}[e] (pm/V)	Solvatochromism[f] (nm)						
						1,4-Dioxane	$CHCl_3$	THF	CH_2Cl_2	DMF	DMSO	Δ
R1	-	266	147.5	145	562	620	674.5	643	668	663	670	50
M1	104	277	127.5	113	289	643.5	691	648	680.5	664	669.5	26
FTC	-	263	-	-	-	629	687	643	647	655	668	39

[a]Glass transition temperature. [b]The 5% weight loss temperature. [c]The best poling temperature. [d]The temperature at which d_{33} values decreased to its 80%. [e]The d_{33} values (NLO performance); [f]The maximum absorption wavelength (λ_{max}, nm) in different solvents (0.02 mg mL^{-1}), Δ=λ_{max} (in DMSO) - λ_{max} (in Dioxane)； Dielectric constant of solvents: 1,4-Dioxane = 2.2; $CHCl_3$= 4.8; THF = 7.5; CH_2Cl_2= 8.9; DMF = 37.6; DMSO = 46.7.

and **M1**. Compared **R1** and **M1** with pure FTC chromophore, the λ_{max}s of **R1** and **M1** in CH_2Cl_2 solvent exhibited large red-shift, as shown in Figure 5. Similar red-shift of λ_{max} of FTC moieties in CH_2Cl_2 also existed in our previous work. [9] This might be due to the influence of the linking groups on the waists of FTC moieties, which changed the conjugated structure of FTC moieties.

There were three acting forces on FTC moieties in the solvents: intermolecular interaction between NLO molecules, interaction between NLO molecules and solvent molecules and intramolecular interaction between chromophore moieties in NLO molecules. Owing to the low concentration of solvent of NLO molecules (0.02 mg mL^{-1}), the intermolecular interaction between NLO molecules could be ignored. Obviously, intramolecular interactions between chromophore moieties were related to the molecular structure which influenced the distribution of FTC moieties and the dipole-dipole interactions. Interestingly, interactions between NLO molecules and solvent molecules were also related to molecular structures. Different molecular structures had different shielding effect on FTC moieties, which could weaken the influence of polarity solvents partly and decrease the redshift of λ_{max}s. After making a detailed comparison of λ_{max} in different solvents, some interesting results could be found. In low-polarity solvents, such as 1,4-dioxane, the interaction between NLO molecules and solvent molecules was very weak and the influence of molecular structures was very obvious. The λ_{max} of **R1** was about 20 nm blue-shifted than that of **M1** and about 10 nm blue-shift than that of pure FTC chromophore under the acting force of intramolecular interaction between two FTC moieties. On the contrary, in high-polarity solvent of DMSO, the interactions between NLO molecules and solvent molecules were so strong that the influence of acting force of intramolecular interaction could not be observed. The λ_{max}s of **R1** and **M1** were almost the same and the influences of structures were submerged. In this paper, Δ value, the difference between the λ_{max}s in DMSO and 1,4-Dioxane, was introduced to evaluate the influence of molecular structures. As shown in Table 1, the Δ values of the FTC moieties in pure FTC chromophore, **R1** and **M1** were 39, 50 and 26 nm, respectively, which could be listed as: **R1**> pure FTC>**M1**. The Δ value of **M1** was smaller than that of pure FTC chromophore, showing the shielding effect on chromophore moieties from each other. Interestingly, the Δ value of **R1** (50 nm) was much larger than that of **M1** (26 nm) although they had similar structures were similar, indicating that the strong intramolecular dipole-dipole interactions existed between two pieces of FTC moieties possibly due to the rigid ringlike structure.

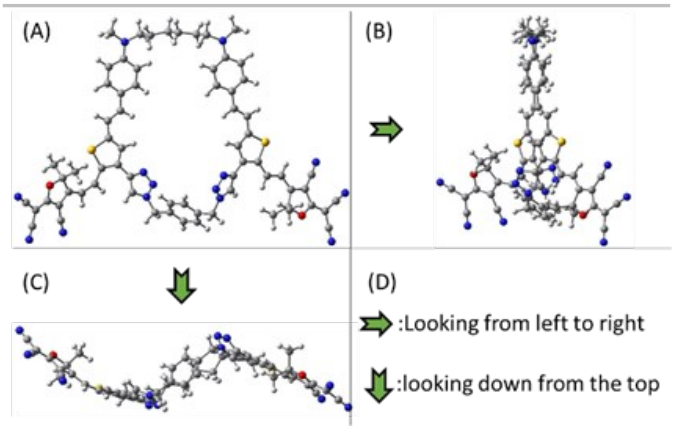

Fig. 6 Optimized chemical structures of **R1**.

Spatial geometry

The spatial geometry of **R1** and **M1** was obtained from the semi-empirical quantum chemistry method (Figure 6 and Figure S6). In order to simplify the calculation, the hexyl group was replaced by the methyl one. Theoretically, in **M1**, the FTC moieties trended to the reverse parallel arrangement due to the strong intramolecular dipole-dipole interactions. As a matter of fact, two FTC moieties were mutually-perpendicular interspersion in space (Figure S6), possibly due to the isolation group between the two FTC moieties. In **R1**, the two FTC moieties had similar direction because the two linkages on the donor and waist positions locked them tightly. However, the direction was not precisely the same with a pretwist angle existed because of the very strong intramolecular dipole-dipole interactions. Theoretically, the atoms of the conjugated structure of FTC moieties were coplanar, just as the same to the structure of **M1** (Figure S6). But the conjugated structure of **R1** had a certain degree of distortion, as shown in the structure of **R1** (Figure 6), as the balanced result of the constraint from the linkages and the strong dipole-dipole interactions between the two FTC moieties, which was in consistent with the experimental results of solvatochromism measurement.

NLO properties

To evaluate their NLO activity, the poled thin films of **R1** and **M1** were fabricated through the convenient spin-coating process. Thanks to their good film-forming properties, high quality thin films were obtained with the thickness in the range of 90 to 150 nm. The most convenient technique to study the second-order NLO activity is to investigate the second harmonic generation (SHG) processes characterized by d_{33}, an SHG coefficient. The method for the calculation of the SHG coefficients (d_{33}) for the poled films has been reported in literatures and our previous papers. [9,10]

From the experimental data, the d_{33} values of **R1** and **M1** were calculated to be 562 and 289 pm/V, respectively, at the fundamental wavelength of 1950 nm (Table 1). To check the reproducibility, we repeated the measurements at least three times and got similar results. Obviously, the d_{33} value of **R1** was much larger than that of **M1**, about two times, regardless of their similar loading density of FTC moieties. This should be ascribed to the superiority of designed rigid ringlike structure, which could promote the conversion from microcosmic large β values of FTC chromophores to the macroscopic second order NLO coefficient of poled films effectively.

Figure 7 exhibited the SHG real-time measuring and testing system, and the real-time SHG signals of films at different temperatures could be detected. In the poling process, a fresh film was placed in the work table while the electric field was on. However, in the depoling

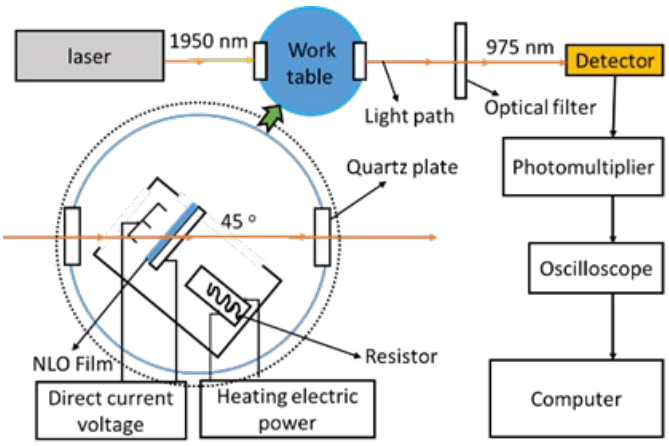

Fig. 7 Schematic diagram of poling device.

process, a poled film was used, and the electric field was off. Real-time relative d_{33} values were calculated based on real-time SHG signals. Poling and depoling schematic diagram was shown in Figure S1A. Poling and decay curves of **R1** and **M1** were shown in Figure 8. As shown in the poling curves (Figure 8 (A)), the real-time SHG signals started to increase at about 60 °C and reached the largest values at specific temperatures, which were named as best poling temperatures. At higher temperatures, the signals began to decrease. The temperature at which d_{33} values decreased to its 80% was used to evaluate the temporal stability, named as $T_{80\%}$.[9,10]

The data of best poling temperatures and temporal stabilities were summarized in Table 1. The best poling temperature of **R1** was very high (147.5 °C), much higher (20 °C) than that of **M1**. Some simple analysis on molecular motion shown in Figure 8 could do some explanation. The rotation diagram of rigid ringlike molecule **R1** and flexible molecule **M1** was shown in Figure 8 (C): in **M1**, thanks to the flexible structure, the FTC moieties of **M1** could revolve round the chemical chain connecting the waists of the two FTC moieties, but that of rigid ringlike molecule **R1** couldn't. The $T_{80\%}$ of **R1** was very high (145 °C), much higher (32 °C) than that of **M1**, indicating the good temporal stability of rigid ringlike molecule **R1**. The relaxing diagram of **R1** and **M1** was shown in Figure 8 (D): in the process of relaxing, rigid ringlike molecule **R1** needed to turn whole molecule upside down, while **M1** just needed to do half of it. Besides, due to the ringlike molecule structure, which was almost an idea spherical structure, the dipole-dipole interaction between molecules could be reduced effectively according to "Site Isolation principle".[4] So it was reasonable that **R1** obtained very good temporal stability.

Experimental section

Materials and Instrumentation

Dichloromethane and *N*,*N*-dimethylform amide (DMF) were dried over and distilled from calcium hydride. Anhydrous ethanol were dried over and distilled from sodium metallic. Tetrahydrofuran (THF) was dried over and distilled from K-Na alloy under an atmosphere of dry nitrogen. FTC-1, pure FTC, Compound B and TCF had been previously reported by our group.[9] All other reagents were used as received.

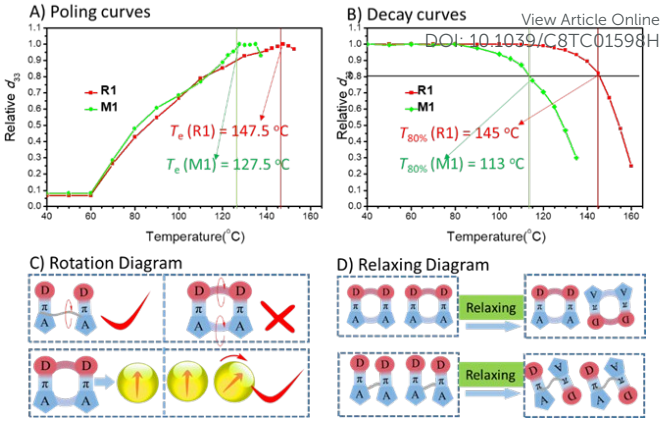

Fig. 8 (A) Poling curves of **R1** and **M1**; (B) Decay curves of **R1** and **M1**; (C) Rotation diagram of R1 and M1: in the structure of **M1**, the FTC part could revolve round the linkage but that of **R1** couldn't; (D) Relaxing diagram of **R1** and **M1**: in the process of relaxing

^{1}H and ^{13}C NMR spectra were measured on a Bruker Advance III (400 MHz) spectrometer using tetramethylsilane (TMS; δ = 0 ppm) as internal standard. Matrix-assisted laser desorption ionization time-of-flight mass spectra were measured on a MALDI-TOF mass spectrometer (MALDI-TOF MS; 5800, AB, SCIEX, American). Elemental analyses (EA) were performed by a CARLOERBA-1106 microelemental analyzer. The Fourier transform infrared (FTIR) spectra were recorded on a PerkinElmer-2 spectrometer in the region of 3000-500 cm^{-1}. The thermal transitions were investigated using a METTLER differential scanning calorimeter DSC822e under nitrogen at a scanning rate of 10 °C/min. The thickness of the films was measured with an Ambios Technology XP-2 profilometer. UV-visible spectra were obtained using a Shimadzu UV-2550 spectrometer. Thermal analysis was performed on NETZSCH STA449C thermal analyzer at a heating rate of 10 °C/min in nitrogen at a flow rate of 50 cm^3/min for thermogravimetric analysis (TGA).

Synthesis

Compound **7**. Under an atmosphere of nitrogen, a solution of compound **6** (2.0 g, 1.1 mmol) and potassium carbonate (150 mg, 1.1 mmol) in C_2H_5OH (20 mL) was stirred at room temperature for 1 h. Then the solution was condensed via rotary evaporation. The resultant crude product was purified by column chromatography with DCM/PE (1:1) as an eluent to give a red solid (0.8 g, 97%). ^{1}H NMR (400 MHz, $CDCl_3$, 298 K), δ (TMS, ppm): 10.02 (s, 2H, -CHO), 7.35-7.33 (d, *J*=8Hz, 4H, ArH), 7.07-6.85 (m, 6H, -CH=, ArH), 6.61-6.59 (d, *J*=8 Hz, 4H, ArH), 3.42 (s, 2H, -CH≡), 3.32-3.27 (m, 8H, -CH_2-), 1.58 (m, 4H, -CH_2-), 1.39 (m, 4H, -CH_2-), 1.32 (m, 12H, -CH_2-), 0.90-0.88 (m, 6H, -CH_3).

Compound **8**. Under an atmosphere of nitrogen, a solution of compound **7** (96.4 mg, 0.127 mmol), compound **B** (24 mg, 0.127 mmol), copper sulfate pentahydrate (320 mg, 1.28 mmol), sodium bicarbonate (215 mg, 2.56 mmol), sodium L-ascorbate (480 mg, 2.56 mmol) in THF/H_2O (80/16 mL) was stirred slowly at 28 °C for 3 h. Then the reaction mixture was condensed via rotary evaporation. The rest aqueous phase was poured out,

and the resultant crude product was purified by column spectroscopy on silica gel using CH_2Cl_2/PE (1:1) as eluent to give a red solid (20 mg, 16.6%). ^{1}H NMR (400 MHz, $CDCl_3$, 298 K), δ (TMS, ppm): 10.47 (s, 2H, -CHO), 7.81 (s, 2H, ArH), 7.35 (s, 4H, ArH), 7.30-7.28 (d, *J*=8Hz, 4H, ArH), 7.08 (s, 2H, =CH-), 7.02-6.98 (d, *J*=16Hz, 2H, =CH-), 6.85-6.81 (d, *J*=16Hz, 2H, =CH-), 6.56-6.54 (d, *J*=8Hz, 4H, ArH), 5.60 (s, 4H, -CH_2-), 3.31-3.23 (m, 8H, -CH_2-), 1.55-1.54 (m, 8H, -CH_2-), 1.30 (m, 16H, -CH_2-), 0.91-0.88 (m, 6H, -CH_3).

R1. Under an atmosphere of nitrogen, a solution of compound **8** (68 mg, 0.0719 mmol), TCF (38 mg, 0.19 mmol) and ammonium acetate in C_2H_5OH/DCM (5/1 mL) was stirred at room temperature for 12 h. Then the solution was condensed via rotary evaporation. The resultant crude product was purified by column chromatography with DCM/EA (10:1) as an eluent to give a blue powder (60 mg, 63.8%). ^{1}H NMR (400 MHz, CD_2Cl_2, 298 K), δ (TMS, ppm): 9.05-9.01 (d, *J*=16 Hz, 2H, -CH=), 7.71 (s, 2H, ArH), 7.24 (s, 4H, ArH), 6.99-6.95 (m, 6H, ArH, -CH=), 6.86-6.82 (d, *J*=16 Hz, 2H, -CH=), 6.65-6.61 (d, *J*=16 Hz, 2H, -CH=), 6.53-6.51 (d, *J*=8Hz, 4H, ArH), 5.55 (s, 4H, -CH_2-), 3.27-3.19 (m, 8H, -CH_2-), 1.76 (s, 6H, -CH_3), 1.50-1.48 (m, 8H, -CH_2-), 1.24 (m, 16H, -CH_2-), 0.83-0.75 (m, 6H, -CH_3). ^{13}C NMR (100 MHz, CD_2Cl_2, 298 K), δ (ppm): 179.4, 175.0, 152.5, 147.9, 143.6, 138.9, 136.3, 135.1, 130.5, 128.9, 128.8, 128.7, 128.3, 124.0, 122.1, 113.7, 112.5, 112.2, 111.8, 111.3, 109.5, 97.2, 51.0, 50.8, 31.6, 27.3, 27.2, 26.7, 26.4, 22.6, 13.8. $C_{78}H_{78}N_{14}O_2S_2$ (EA) (%, found/calcd): C, 71.35/71.64; H, 6.01/6.01; N, 14.86/15.00; S, 4.88/4.90. MS (MALDI-TOF): m/z for $C_{78}H_{78}N_{14}O_2S_2$ (found/calcd): $[M+Na]^+$: 1329.5/1329.0.

M1. Under an atmosphere of dry nitrogen, a solution of **FTC-5** (130 mg, 0.21 mmol), compound **B** (20 mg, 0.108 mmol), copper sulfate pentahydrate (10% mmol), sodium bicarbonate (20% mmol), sodium L-ascorbate (20% mmol) in 5/1 mL of THF/H_2O was stirred at 28-30 °C for 3 hrs. Then the reaction mixture was poured into water and extracted with CH_2Cl_2 for three times (50 mL×3). The combined organic solution was dried over anhydrous sodium sulfate and condensed via rotary evaporation. The residue was purified by column spectroscopy on silica gel using the solvents of CH_2Cl_2/ethyl acetate (2:1) as eluent to give a blue powder (120 mg, 82.1%). ^{1}H NMR (400 MHz, CD_2Cl_2, 298 K), δ (TMS, ppm): 8.67-8.63 (d, *J*=16 Hz, 2H, -CH=), 7.74 (s, 2H, ArH), 7.41 (s, 4H, ArH), 7.19-7.17 (d, *J*=8 Hz, 4H, ArH,), 6.80-6.78 (d, *J*=8 Hz, 2H, -CH=), 6.69-6.63 (m, 6H, ArH, -CH=), 6.54-6.51 (d, *J*=12 Hz, 4H, ArH), 6.39-6.35 (d, *J*=16 Hz, 2H, -CH=), 5.52 (s, 4H, CH_2-), 3.25-3.21 (m, 8H, -CH_2-), 1.6 (s, 6H, -CH_3), 1.52 (m, 8H, -CH_2-), 1.25 (m, 16H, -CH_2-), 0.83 (m, 12H, -CH_3). ^{13}C NMR (100 MHz, CD_2Cl_2, 298 K), δ (ppm): 175.8, 173.7, 152.4, 149.3, 142.7, 139.5, 138.5, 135.6, 135.1, 132.2, 129.3, 129.0, 125.7, 122.7, 121.9, 114.3, 112.4, 112.0, 111.8, 111.8, 111.6, 97.8, 94.9, 54.7, 50.9, 31.7, 27.2, 26.7, 26.1, 22.7, 13.8. $C_{84}H_{92}N_{14}O_2S_2$ (EA) (%, found/calcd): C, 72.14/72.38; H, 6.63/6.65; N, 14.04/14.07; S, 4.45/4.60. MS (MALDI-TOF): m/z for $C_{84}H_{92}N_{14}O_2S_2$ (found/calcd): $[M+K]^+$: 1431.6/1431.0.

Preparation of Thin Films

The two molecules were dissolved in THF (concentration, 4 wt %) and the solutions were filtered through syringe filters. Then the solutions were spin-coated onto indium-tin-oxide (ITO)-coated glass substrates and the ITO glasses were cleaned by DMF, acetone, distilled water and THF sequentially in ultrasonic bath before use. Residual solvent was removed by heating the films in a vacuum oven at 40 °C for 8 hrs.

NLO Measurement of Poled Films

Schematic diagram of poling device was shown in Figure 7. The second-order nonlinear optical (NLO) efficiencies of the compounds were measured by in situ second harmonic generation (SHG) experiment using a closed temperature controlled oven with optical windows and three needle electrodes. The films were kept at 45° to the incident beam and poled inside the oven and the conducting planes faced to the laser. Then the laser was lighted and the SHG intensity was monitored simultaneously. The poling temperatures of the five kinds of films were different. They shared the same other poling conditions: gap distance, 0.8 cm; voltage, 7.0 kV at the needle point. 1950 nm laser radiation was used to investigate the NLO efficiencies. The doubled frequency signals, which were 975 nm, were detected by an Andor's DU420A-BR-DD CCD after the mixed signals passed through the monochromator and a customized Y-cut quartz crystal served as the reference.

Conclusions

In this work, two second-order nonlinear optical (NLO) molecules based on FTC chromophore, **R1** and **M1**, had been designed and synthesized. **R1** was a rigid ringlike structure molecule and **M1** was a flexible molecule and used for comparison. They both exhibited good thermal stabilities, with decomposition temperatures higher than 260 °C. Excitingly, **R1** possessed very large NLO activity, with the highest d_{33} value of 562 pm V^{-1} at 1950 nm, which was nearly two times that of **M1**. Besides, the temporal stability of **R1** was very good, with its $T_{80\%}$ as high as 145 °C. These results proved that the excellence of rigid ringlike structure was an ideal spherical structure conforming the "Site Isolation principle".

Conflicts of interest

There are no conflicts to declare.

Acknowledgements

This work was supported by the National Natural Science Foundation of China (No. 21734007).

Notes and references

1 (a) D. Yu, A. Gharavi and L. Yu, *J. Am. Chem. Soc.*, 1995, **117**, 11680; (b) T. Marks and M. Ratner, *Angew. Chem. Int. Ed.*, 1995, **34**, 155; (c) S. Marder, B. Kippelen, A. Jen and N. Peyghambarian, *Nature*, 1997, **388**, 845; (d) J. Luo, M. Haller,

H. Ma, S. Liu, T. Kim, Y. Tian, B. Chen, S. Jang, L. Dalton and A. Jen, *J. Phys. Chem. B*, 2004, **108**, 8523; (e) Y. Shi, C. Zhang, H. Zhang, J. Bechtel, L. Dalton, B. Robinson and W. Steier, *Science*, 2000, **288**, 119; (f) Y. Bai, N. Song, J. Gao, X. Sun, X. Wang, G. Yu and Z. Wang, *J. Am. Chem. Soc.*, 2005, **127**, 2060; (g) Y. Liao, C. Anderson, P. Sullivan, A. Akelaitis, B. Robinson and L. Dalton, *Chem. Mater.*, 2006, **18**, 1062; (h) X. Ma, R. Liang, F. Yang, Z. Zhao, A. Zhang, N. Song and Q. Zhang, *J. Mater. Chem*., 2008, **18**, 1756; (i) J. Luo, X. Zhou and A. Jen, *J. Mater. Chem.*, 2009, **19**, 7410; (j) Z. Li, W. Wu, G. Yu, Y. Liu, C. Ye, J. Qin and Z. Li, *ACS Appl. Mater. Inter.*, 2009, **1**, 856; (k) Z. Li, G. Yu, W. Wu, Y. Liu, C. Ye, J. Qin and Z. Li, *Macromolecules*, 2009, **42**, 3864; (l) L. Dalton, P. Sullivan and D. Bale, *Chem. Rev.*, 2010, **110**, 25; (m) L. Dalton, D. Lao, B. Olbricht, S. Benight, D. Bale, J. Davies, T. Ewy, S. Hammond and P. Sullivan, *Opt. Mater.*, 2010, **32**, 658; (n) J. Luo, S. Huang, Z. Shi, B. Polishak, X. Zhou and A. Jen, *Chem. Mater.*, 2011, **23**, 544; (o) Z. Li, W. Wu, C. Ye, J. Qin and Z. Li, *Polymer*, 2012, **53**, 153; (p) W. Wu, Q. Huang, G. Qiu, C. Ye, J. Qin and Z. Li, *J. Mater. Chem.*, 2012, **22**, 18486; (q) J. Liu, L. Wang, Z. Zhen, X. Liu, *Colloid Polym. Sci.*, 2012, **290**, 1215; (r) J. Luo and A. Jen, IEEE J SEL TOP QUANT, 2013, **19**, 3401012; (s) J. Wu, J. Luo, N. Cernetic, K. Chen, K. Chiang and A. Jen, J. *Mater. Chem. C*, 2016, 4, 10286; (t) D. Chen, C. Zhong, Y. Zhao, L. Nan, Y. Liu, and J. Qin, *J. Mater. Chem. C.*, 2017, **5**, 5199; (u) Y. Yang, J. Liu, H. Xiao, Z. Zhen and S. Bo, *Dyes and Pigments*, 2017, **139**, 239; (v) Z. Li, P. Chen, Y. Xie, Z. Li and J. Qin, *Adv. Electron. Mater*., 2017, **3**, 1700138; (w) J. Wu, B. Wu, W. Wang, K. Chiang, A. Jen, J. Luo, *Mater. Chem. Front*., 2018, **2**, 901; (x) Z. Li, Z. Li, *Acta. Polym. Sin*., 2017, **2**, 155.

2 (a) T. Kim, J. Kang, J. Luo, S. Jang, J. Ka, N. Tucker, J. Benedict, L. Dalton, T. Gray, R. Overney, D. Park, W. Herman and A. Jen, *J. Am. Chem. Soc.*, 2007, **129**, 488; (b) M. Ronchi, A. Biroli, D. Marinotto, M. Pizzotti, M. Ubaldi and S. Pietralunga, *J. Phys. Chem. C*, 2011, **115**, 4240; (c) D. Knorr, S. Benight, B. Krajina, C. Zhang, L. Dalton and R. Overney, *J. Phys. Chem. B*, 2012, **116**, 13793.

3 (a) J. Zyss and I. Ledoux, *Chem. Rev.*, 1994, **94**, 77; (b) Q. Li, C. Lu, J. Zhu, E. Fu, C. Zhong, S. Li, Y. Cui, J. Qin and Z. Li, *J. Phys. Chem. B*, 2008, **112**, 4545.

4 (a) B. Robinson, L. Dalton, A. Harper, A. Ren, F. Wang, C. Zhang, G. Todorova, M. Lee, R. Aniszfeld, S. Garner, A. Chen, W. Steier, S. Houbrecht, A. Persoons, I. Ledoux, J. Zyss and A. Jen, *Chem. Phys*., 1999, **245**, 35; (b) L. Dalton, W. Steier, B. Robinson, C. Zhang, A. Ren, S. Garner, A. Chen, T. Londergan, L. Irwin, B. Carlson, L. Fifield, G. Phelan, C. Kincaid, J. Amend and A. Jen, *J. Mater. Chem.*, 1999, **9**, 1905; (c) B. Robinson and L. Dalton, *J. Phys. Chem. A*, 2000, **104**, 4785.

5 Z. Li, Q. Li and J. Qin, *Polym. Chem.*, 2011, **2**, 2723.

6 (a) H. Ma, S. Liu, J. Luo, S. Suresh, L. Liu, S. Kang, M. Haller, T. Sassa, L. Dalton and A. Jen, *Adv. Funct. Mater*, 2002, **12**, 565; (b) Z. Li, Z. Li, C. Di, Z. Zhu, Q. Li, Q. Zeng, K. Zhang, Y. Liu, C. Ye and J. Qin, *Macromolecules*, 2006, **39**, 6951; (c) Q. Zeng, Z. Li, Z. Li, C. Ye, J. Qin, B. Tang, *Macromolecules*, 2007, **40**, 5634; (d) W. Wu, Y. Fu, C. Wang, C. Ye, J. Qin and Z. Li, *Chem. Asian J.*, 2011, **6**, 2787; (e) W. Wu, C. Ye, J. Qin and Z. Li, *ACS Appl. Mater. Interfaces*, 2013, **5**, 7033; (f) W. Wu, L. Huang, Y. Fu, C. Ye, J. Qin and Z. Li, *Chin. Sci. Bull.*, 2013, **58**, 2753; (g) R. Tang, H. Chen, S. Zhou, W. Xiang, X. Tang, B. Liu, Y. Dong, H. Zeng and Z. Li, *Polym. Chem.*,2015, **6**, 5580; (h) R. Tang, S. Zhou, Z. W. Xiang, Y. Xie, H. Chen, Q. Peng, G. Yu, B. Liu, H. Zeng, Q. Li and Z. Li, *J. Mater. Chem. C*, 2015, **3**, 4545; (i) G. Liu, P. Chen, R. Tang and Z. Li, *Sci. China Chem*., 2016, **59**, 1561; (j) R. Tang, S. Zhou, Z. Cheng, G. Yu, Q. Peng, H. Zeng, G. Guo, Q. Li and Z. Li, *Chem. Sci.*,2017, **8**, 340; (k) R. Tang and Z. Li, *Chem. Rec.*, 2017, 17, 71; (k) P. Chen and Z. Li, *Chin. J. Polym. Sci.*, 2017, **35**, 793.

7 Y. Liao, K. Firestone, S. Bhattacharjee, J. Luo, M. Haller, S. Hau, C. Anderson, D. Lao, B. Eichinger, B. Robinson, P. Reid, A. Jen and L. Dalton, *J. Phys. Chem. B*, 2006, **110**, 5434.

8 L. Dalton, A. Harper, A. Ren, F. Wang, G. Todorova, J. Chen, C. Zhang and M. Lee, *Ind. Eng. Chem. Res*. 1999, **38**, 8.

9 P. Chen, X. Yin, Y. Xie, S. Li, S. Luo, H. Zeng, G. Guo, Q. Li and Z. Li, *J. Mater. Chem. C*, 2016, **4**, 11474.

10 (a) Z. Li, W. Wu, Q. Li, Gui Yu, L. Xiao, Y. Liu, C. Ye, J. Qin and Z. Li, *Angew. Chem. Int. Ed*., 2010, **49**, 2763; (b) W. Wu, G. Yu, Y. Liu, C. Ye, J. Qin and Z. Li, *Chem. Eur. J*., 2013, **19**, 630.

View Article Online
DOI: 10.1039/C8TC01598H

TOC

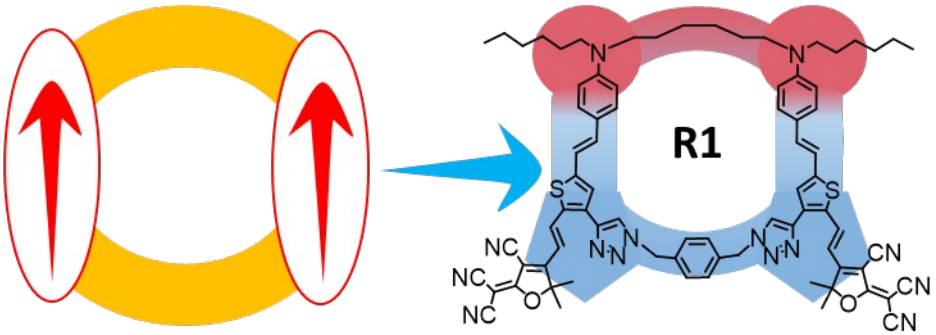

Ringlike molecule **R1** containing two FTC moieties exhibited good thermal stability and excellent EO performance, with an ultrahigh d_{33} value of 562 pm V^{-1} @1950 nm and a high $T_{80\%}$ at 145 °C.